Hydration of Passive Oxide Films on Aluminum

B. C. Bunker,* G. C. Nelson, K. R. Zavadil, J. C. Barbour, F. D. Wall, and J. P. Sullivan

Sandia National Laboratories, Albuquerque, New Mexico 87185

C. F. Windisch Jr., M. H. Engelhardt, and D. R. Baer

Pacific Northwest National Laboratory, Richland, Washington 99352

Received: August 22, 2001; In Final Form: February 14, 2002

Secondary ion mass spectrometry (SIMS) has been used in conjunction with isotopic labeling to determine the extent and rate of passive film hydration on aluminum. The rates at which oxygen- and hydrogen-containing species migrate through the film have been determined as a function of temperature and applied potential (cathodic and anodic polarization). The results suggest that defects such as hydroxide ions are prevalent and mobile in the oxide film, influencing the kinetics and mechanisms of corrosion and pitting processes.

Introduction

This paper involves the use of secondary ion mass spectrometry (SIMS) to determine the hydration state of thin native oxide films on aluminum. Understanding the hydration state of the native oxide is important for mechanisms that have been proposed to explain the corrosion and pitting of passivated metals. Below is a brief description of models for the pitting and corrosion of aluminum and a discussion of how hydration of the native oxide could contribute to both processes. This is followed by results showing how SIMS depth profiles have been utilized to monitor oxide hydration processes.

Pitting of Aluminum. The exceptional corrosion resistance of aluminum is critically dependent on the presence of a passive oxide film that is formed on its surface.[1] For passive metals such as aluminum and stainless steel, the most common form of corrosion is pitting, which involves a localized breakdown of the oxide film.[2] Although pit initiation is a localized phenomenon, the transport of species through the passive oxide may control pit initiation kinetics. It is known that pitting only occurs when an anodic potential exceeding the pitting potential is applied across the oxide. In the "point defect" model for pitting[3,4] (Figure 1), it is postulated that anodic polarization is required to drive anionic defects such as aluminum vacancies through the film to the Al:Al_2O_3 interface, while cationic species such as oxygen vacancies are driven to the Al_2O_3:solution interface. This is equivalent to moving Al^{3+} toward the solution interface while O^{2-} is driven toward the Al. Pitting is thought to occur when the flux of aluminum vacancies reaching the Al:Al_2O_3 interface exceeds the rate at which Al is oxidized to Al^{3+} to fill the vacancies. The vacancies are then assumed to nucleate and grow localized voids that undermine the overlaying oxide and eventually form pits. Environmental species known to promote pitting such as the chloride ion are assumed to substitute for oxygen in the lattice, creating defects in the Al_2O_3 that increase the concentration and flux of aluminum vacancies through the film.

While defect migration may be required for pitting, quantitative predictions of initiation kinetics are not consistent with published literature regarding how easy it is to create and move

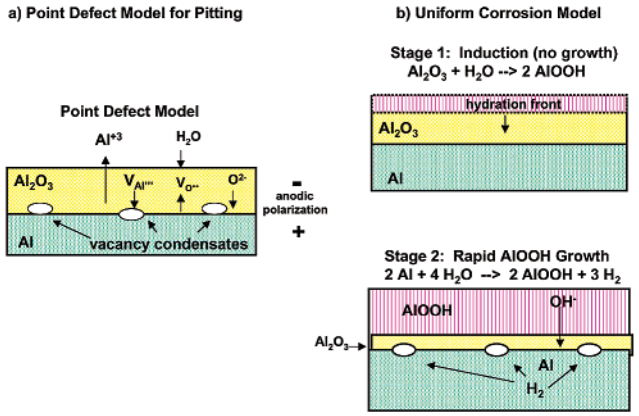

Figure 1. (a) Point defect model for the pitting of Al. Under anodic polarization, aluminum ions are driven to the Al_2O_3:solution interface and into solution, while aluminum vacancies are driven to the Al:Al_2O_3 interface where they aggregate to form voids as precursors to pits. Oxygen ions are also driven to the Al:Al_2O_3 interface, while oxygen vacancies migrate to the Al_2O_3:water interface to be filled by water molecules. (b) Model for uniform corrosion of Al in hot water. An induction time in which no corrosion is apparent is associated with the hydration of the native oxide. Hydration eventually leads to enhanced diffusion and rapid film growth. The hydrated oxide is predominantly AlOOH except at the Al:Al_2O_3 interface, where the hydroxide is reduced by Al to regenerate the oxide and generate H_2.

aluminum or oxygen vacancies in aluminum oxide. In sapphire, the activation energy for creating aluminum vacancies is high (between 10 and 30 eV[5]). Equilibrium concentrations for "intrinsic" aluminum vacancies are estimated to be less than $1/cm^3$ at room temperature (orders of magnitude lower than impurity levels in even ultrapure materials). Extrapolations of tracer diffusion studies in sapphire[6] to room temperature indicate that aluminum and oxygen vacancy diffusion is negligible ($D = 10^{-80}$ cm^2/s). Such defect diffusion coefficients are many orders of magnitude slower than those required to be consistent with known pitting kinetics ($D = 10^{-20}$ cm^2/s in the absence of an applied field). It is estimated that vacancy migration can be increased by a factor of 10^6-10^7 by the pitting potential (application of 500 mV across a 5 nm film introduces a field gradient of 10^6 V/cm across the oxide).[3] High fields (approaching breakdown voltages) could also stimulate the formation of

* To whom correspondence should be sent. E-mail: bcbunke@sandia.gov.

10.1021/jp013246e CCC: $22.00
Published on Web 04/11/2002

defects such as those seen in the electron-beam assisted oxidation of Al and the enhanced conductivity[7] of radiation-damaged Al_2O_3. However, it is difficult to see how such effects could bridge the over 60 order of magnitude gap between defect transport rates seen in bulk alumina and rates inferred for transport in the native oxide.

It appears that the structure and properties of the native oxide must be substantially different than those of bulk α-Al_2O_3 (in which Al^{3+} occupies two-thirds of the octahedral sites in a hexagonal close-packed oxygen array) in order to rationalize observed pitting kinetics. One explanation[8] for the apparent enhancement in defect diffusion in the native oxide relative to α-Al_2O_3 is that the amorphous oxide has a structure resembling that of highly defective γ-Al_2O_3 (depicted using the spinel formula υAl_8O_{12}, in which υ represents an aluminum vacancy). Of the eight aluminum cations in the formula unit, six are assumed to occupy octahedral sites with the other two occupying tetrahedral sites. Since the aluminum vacancy also involves a tetrahedral site, vacancy transport among the available tetrahedral sites (one-third of which are vacant) might be facile relative to α-Al_2O_3.

A second intriguing possibility is that the defects responsible for pitting are not those identified in the current point defect model but are defects created in the film as a result of environmental exposure. The fact that the electrical conductivity of passive oxide films on Al can be increased by over a factor of 10^6 by exposing the films to water[9] suggests that the defect chemistry of the film is highly sensitive to environmental factors. Proponents of the γ-Al_2O_3 structure for the native oxide suggest that water can be incorporated into the oxide lattice while preserving the spinel structure for $Al_2O_3-nH_2O$ compositions ranging up to $n = 0.6$.[8] For $n < 0.2$, the protons incorporated into the spinel structure (as hydroxide ions) serve to fill aluminum vacancies. At $n = 0.2$, the spinel (having the composition HAl_5O_8) is "defect-free". From $0.2 < n < 0.6$, additional protons are accounted for as "interstitial" hydrogen, representing a different defect type within the spinel structure. Studies of the uniform corrosion of aluminum in hot water suggest that water can also react with the native oxide to create oxyhydroxide and hydroxide phases on the aluminum surface whose properties are substantially different than those of the parent oxide. The motivation for this investigation is to try to understand the extent to which water modifies the structure and composition of the passive films and whether such modifications might influence phenomena such as pitting and corrosion.

Hydration of Thin Oxide Films in Corrosion. For a dense oxide such as Al_2O_3, hydration primarily involves the disruption of Al−O−Al bonds via hydrolysis to form Al−OH species. In hydrolysis, one Al−O−Al linkage is broken to form two Al−OH for each water molecule consumed. The hydrolysis process can modify the oxide lattice by lowering its effective "cross-link density" and replacing O^{2-} ions with more mobile species. These species include protons, which can hop from oxygen to oxygen as in proton conductors,[10] the hydroxide ions themselves, which can readily migrate between oxygen vacancies, and water molecules, which can fill interstices in the structure that are opened up during hydration. Species such as the hydroxide ion are anionic defects that could be driven to the Al:Al_2O_3 interface under an applied anodic potential. Extensive hydration eventually produces oxyhydroxide or hydroxide phases such as AlOOH and $Al(OH)_3$ that are thermodynamically more stable than Al_2O_3 at room temperature.[11] Such phases are commonly observed in the uniform corrosion of aluminum in hot water.[14] The rate of growth of oxyhydroxide and hydroxide scales is reported to proceed in three stages:[14] (1) an induction period (of minutes to hours depending on temperature) during which no growth is observed (the thermal oxide does not change in thickness), (2) a period of rapid growth during which a pseudoboehmite (AlOOH) layer forms and grows to a thickness of several microns, and (3) a period of slower growth in which $Al(OH)_3$ grows on top of the pseudoboehmite.

The ability of passive films to function as diffusion barriers is expected to be strongly dependent on the extent of film hydration. While diffusion coefficients for oxygen and hydrogen have not been measured for the hydrated phases, the activation energy for D−H exchange within boehmite is estimated to be only 0.7 eV.[12] Ion motion in boehmite is thought to resemble that seen for ice (the ultimate hydrated solid). In ice, diffusion coefficients and activation energies for the diffusion of oxygen and hydrogen are identical[13] (at around 3×10^{-11} cm^2/sec at -10 °C and 0.6−0.7 eV, respectively). While diffusion through the hydrated passive oxide is not anticipated to be this rapid, it could be substantially faster than it is in the parent oxide. The induction period for the uniform corrosion of aluminum could correspond to the time required for a hydration front to move through the native oxide, compromising its ability to function as a diffusion barrier (Figure 1b).

While hydrolysis reactions create hydroxyl groups, other reactions can eliminate hydroxide ions and regenerate oxide structures. Within the bulk oxide, condensation reactions can occur in which two hydroxide ions recombine to generate an oxide linkage and a water molecule (the reverse of hydrolysis). At the Al:Al_2O_3 interface, hydroxide ions and water can also be eliminated by electrochemical reactions in which the aluminum metal is oxidized and the protons are reduced to form hydrogen gas. (Aluminum hydroxide phases are known to be thermodynamically unstable in contact with aluminum metal.[15]) Such hydrogen-generating reactions are similar to what happens when water encounters clean Al surfaces.[16] The role of Al in electrochemically "healing" hydration-induced damage may be critical to preserving the passive film as a diffusion barrier. The role of species such as Cl^- in promoting pitting may involve the occupation of sites within the oxide that interfere with condensation and other oxide-regenerating processes.

The uniform corrosion rate, as reflected by the steady state thickness and hydration state of the oxide on Al immersed in water, should be strongly dependent on the relative rates of the above reactions. Extremes in behavior include no apparent corrosion (negligible hydration and film growth) as seen in humid air, extensive hydroxide formation and hydrogen evolution, as indicated by Alwitt's studies in hot water,[14] and growth of an oxide rather than a hydroxide film, which occurs when the rate of transport and annihilation of hydroxide at the Al:Al_2O_3 interface (to generate H_2) exceeds the rate of network hydrolysis at the Al_2O_3:solution interface as seen in high-voltage anodization.[17]

Oxide hydration could also contribute to nonuniform corrosion or pitting due to the creation film stresses and the generation of hydrogen gas at the Al:Al_2O_3 interface. Hydrogen can diffuse through both Al and Al_2O_3.[18] However, if the H_2 is generated at the Al:Al_2O_3 interface faster than it can diffuse away, the hydrogen will nucleate and grow gas bubbles. In the "hydrogen bubble" model for pitting, it is assumed that the pitting potential corresponds to voltage required to drive hydroxide ions to the Al:Al_2O_3 interface fast enough to promote bubble nucleation. The bubbles could eventually generate sufficient pressure to

blow holes through the passive film and initiate pits. Hydrogen bubbles might resemble the voids reported by MacDonald and others.[4]

The "hydrogen bubble" model is just one example of a sequence of events where environmental interactions could restructure the passive film and promote either pitting or uniform corrosion. To validate such models, experimental results are needed that can determine the rate and extent of oxide hydration and how rapidly species such as O^{2-}, OH^-, H^+, and Cl^- migrate through the film under a range of polarization conditions. However, it is difficult to obtain compositional information on the native oxide, which is typically 3−6 nm thick. Secondary ion mass spectrometry (SIMS) is one of the few techniques that is well suited to performing such studies. The purpose of this paper is to illustrate the utility of SIMS in investigating reactions in thin passive films on metals.

Secondary Ion Mass Spectrometry in Oxide Hydration Studies. SIMS is a technique that provides compositional depth profiles by sputtering surfaces using ion beams and analyzing the yield of selected sputtered ions as a function of time. SIMS is one of the few techniques having sufficient depth resolution to provide elemental depth profiles for the native oxide.[19] SIMS has the added advantage that it can detect species such as hydroxide ions[20] at lower concentrations (below 100 parts per million) than are typical for many surface analytical methods. A final advantage of SIMS is that reactions between water and the oxide can be monitored using isotopic labeling in either the oxide or the water.[21] Comparing the diffusion or exchange rates of both oxygen and hydrogen labels can help identify whether the mobile species are H^+, OH^-, O^{2-}, or H_2O. For example, if H:D exchange in the film is rapid, but ^{16}O:^{18}O exchange is negligible, then H^+ is implicated as the most mobile species. If H:D and ^{16}O:^{18}O exchange occur at the same rate, OH^- or H_2O are implicated as the most mobile species, while if H:D exchange is negligible relative to ^{16}O:^{18}O exchange, O^{2-} migration is dominant. If the native oxide is labeled with ^{18}O, the labeled region can be used as a marker of the original oxide surface. If processes such as hydration or anodization lead to oxide growth, the relative position of the labeled zone can provide information regarding growth mechanisms. If reactions involving normal water lead to growth of an ^{16}O-labeled zone on top of the ^{18}O marker layer, Al^{3+} is probably moving faster than O^{2-} through the film. If an ^{16}O-enriched oxide forms underneath the original oxide, oxygen transport must be more rapid than Al^{3+} transport. If the ^{18}O marker is completely gone, either film dissolution has been extensive, or there is rapid oxygen exchange between the film and the solution due to reversible hydrolysis reactions.

The utility of SIMS in studying reactions between oxides and water is highlighted in this paper by examining specific reactions that occur when Al metal is exposed to aqueous solutions in different electrolytes under a range of polarization conditions. The SIMS results show that significant hydration of the native oxide does occur and that both H- and O-containing species move through the passive film more rapidly than indicated by either aluminum or oxygen vacancy diffusion studies in bulk α-Al_2O_3.

Experimental Section

Materials. Aluminum samples were high purity single crystals (Electronic Space Products International or Monocrystals, Inc.) having the [111] orientation. Both electropolished and mechanically polished crystals were examined. High-purity polycrystalline Al (99.99%, Johnson Matthey) was also investigated. Some samples were treated in HF solutions to remove the thermal oxide and then reoxidized in air, while some samples were cleaned by mechanical polishing with emery paper. The HF or mechanically polished samples were ultrasonically cleaned prior to use (30 s in deionized water). Samples having ^{18}O-labeled oxides were prepared under ultrahigh vacuum conditions by sputtering with 3 keV Ar^+ ions followed by annealing to 800 K for 10 min. Auger electron spectroscopy was used to confirm the generation of a clean, metallic Al surface. The samples were then transferred to a contiguous high-pressure cell and exposed to $^{18}O_2$ (95% labeled) at 760 Torr for several hours.

Hydration Experiments. Hydration experiments were performed by immersing Al samples in glass beakers containing desired salt solutions (deionized water or 0.05 M NaCl). Experiments were conducted in laboratory air. Solution temperatures were controlled to within +1 °C on a standard stirrer hotplate. Typical solution volumes were 100 mL, but 25 mL volumes were used for experiments involving D_2O (99%, Cambridge Isotope Laboratories, Inc.). A few experiments were conducted in mixtures of D_2O and $H_2{}^{18}O$. Isotopic abundances measured for this labeled water via mass spectrometry were ^{16}O = 74%, ^{18}O = 26%, H = 33%, and D = 67%. For hydration experiments conducted at Sandia, samples were rinsed and transported to the SIMS apparatus in room-temperature D_2O followed by transfer into the UHV sample chamber. At PNNL, hydration and electrochemical experiments were performed in an electrochemical cell attached to a portable ultrahigh vacuum transfer system.[22] With this system, samples could be rinsed and transferred directly into the SIMS apparatus without exposing the samples to ambient conditions.

Electrochemical Testing. Electrochemical experiments were performed at PNNL using a special cell described in previous publications.[23] A Pt wire served as the counter electrode. Most tests were conducted using a Pt pseudoreference electrode. Calibrations of the pseudoreference electrode before and after corrosion experiments indicated that the electrode has a potential of approximately −30 mV relative to a standard calomel electrode. Experiments were conducted in nitrogen-purged 0.05 M NaCl. Some solutions were isotopically labeled as described above. Measurements of potential or current were made using a PAR 273A potentiostat. Potentials for polarization experiments were selected by obtaining current−voltage curves for a given sample type. Actual corrosion experiments were conducted by monitoring the current passed at a fixed potential. After the corrosion test, samples were rinsed and dried in the cell and transferred directly into the SIMS apparatus for analysis.

SIMS Profiling and Calibrations of Depth Profiles. Secondary ion mass spectrometry experiments were performed using PHI TRIFT I time-of-flight mass spectrometers (one at Sandia and one at PNNL). A 15 keV Ga ion beam was used for both sputtering and analysis. The ion beam was typically rastered over a 25 micron × 25 micron area for analysis and a 90 micron × 90 micron area for dc sputtering. For each point in the depth profile, ion yields were measured for 27 s followed by dc sputtering for 5 s for a total analysis time of 32 s per data point.

The sputtering yields of various ions vs time obtained in SIMS analyses can be used to identify the chemical composition of species in the film as a function of depth. For reactions between Al_2O_3 and aqueous solutions, sputtered cations of interest include Al^+ and solution ions such as H^+, Na^+, and K^+. Sputtered anions of interest include O^-, OH^-, and halide ions such as Cl^- and F^-. For SIMS experiments involving the use of

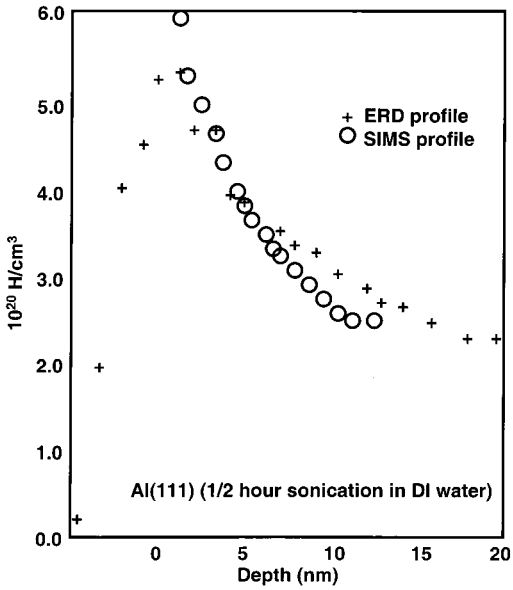

Figure 2. Comparisons between the reference hydrogen depth profile obtained via ERD on a sonicated Al(100) crystal and a SIMS profile obtained on the same sample. Such comparisons have been used to calibrate the SIMS count rate in terms of OH/cm^3.

isotopically labeled oxygen and hydrogen, some species of interest end up having similar masses. (For example, ^{18}OH- and F− both have a mass of 19.) However, the results reported here involve collecting sputtered ion yields for all species within one atomic mass unit unless otherwise stated (see Results and Discussion).

SIMS analyses involve determining the sputtering yields for species of interest as a function of sputtering time. Calibration methods and standards are required to convert the sputtering yield and sputtering time into species concentration and depth scales, respectively, for a known sputtering condition. Here, the depth scale was calibrated by measuring the thickness of the native oxide on Al samples using an ellipsometer and performing SIMS analyses on the same sample. In the SIMS profiles, the thickness of the oxide layer is defined by the sputtering time at which ion yields for species prevalent in the oxide (such as O^-, O_2^-, and AlO^-) drop to 50% of their value in the "bulk". For standard sputtering conditions (spot size and sputter gun current), a sputtering time of 70 s corresponds to an oxide film thickness of 6 nm.

The concentrations of Al- and O-containing species have been calibrated from the sputtering yields obtained on the native oxide, assuming the oxide has the composition Al_2O_3. The concentrations of −OH- and H-containing species have been obtained by performing SIMS analyses on Al samples that were corroded uniformly by exposing the samples to deionized water in an ultrasonic bath for 0.5 h. The ultrasonic cleaning produces a hydrated oxide that is thick enough (as thick as 1 μm) to allow for parallel analyses using elastic recoil detection analyses (ERD) (Figure 2). Rutherford backscattering (RBS) and elastic recoil detection (ERD) analyses for calibrating the depth and concentration scales for the SIMS depth were performed at Sandia using ion beams from a tandem Van de Graff accelerator. ERD profiles were obtained using a 24 MeV $^{28}Si^{5+}$ beam at an angle of incidence of 30°, while the RBS profiles were obtained using a 2.8 MeV He^+ beam at normal incidence.

Sputtering yields in SIMS can vary from day to day, sample to sample, or spot to spot due to variations in sputtering conditions (beam diameter and flux). For this reason, all SIMS results have been calibrated relative to internal standards.

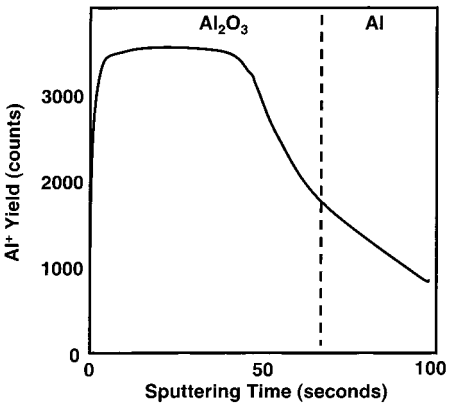

Figure 3. Sputtering yield for Al^{3+} ions from polycrystalline Al covered by a native oxide. Dashed line indicates the position of the Al:Al_2O_3 interface.

Normally, SIMS anion yields were referenced to an O^- ion (mass 16) yield normalized to 10^5 counts. With this normalization, a yield of 1000 counts for mass 17 corresponds to a hydroxyl content of 6×10^{20} OH/cm^3. (If the film is represented by either γ-Al_2O_3 or AlOOH, this yield of 1000 counts corresponds to the protonation of 1% of the oxygens present in the solid.)

Sputtering yields in SIMS can be quite sensitive to the matrix from which the ion was sputtered. This phenomenon is illustrated by the depth profile obtained for the Al^+ ion (m/e = 27) on an Al film covered by a native oxide. Although the Al concentration in Al_2O_3 is less than that in Al (4.7×10^{22} atoms/cm^3 vs 6.0×10^{22} atoms/cm^3), the Al^+ yield for Al_2O_3 is much greater than it is in Al (Figure 3). However, in this paper, it is assumed that the sputtering yields for species within the oxide layer are independent of the hydrogen content of the film (i.e., that oxides and hydroxides exhibit similar sputtering characteristics.) This assumption is based on the observations that (1) the sputtering efficiencies of mass 16 and mass 17 are comparable (near 6×10^{20} O/cm^3 as determined via ERD calibration), and (2) ERD measurements on thin (<5 nm) oxides with a range of hydroxide contents are all consistent with the thick film calibration. (While ERD on the thinnest films are still accurate in terms of the total atoms/cm^2, the depth resolution is insufficient for providing depth profiles.) Another assumption is that the sputtering process itself does not lead to a redistribution of species within the oxide. The similarity of profiles obtained via SIMS and ERD suggests that redistribution is not a serious problem for the oxides examined here.

Chloride ion concentrations have been calibrated by ion implanting Cl into a single-crystal Al(111) sample. A depth profile was calculated for the implant based on the energy and fluence of the ion beam. The maximum concentration of the Cl implant was estimated to be 4 at. % within the bulk Al at a depth of 40 nm. The concentration of Cl within the thermal oxide was estimated to be 0.5 at. %. SIMS profiles obtained on the implanted sample indicate that a normalized yield of 1000 counts for mass 35 corresponds to a concentration of 0.045 at. % within the oxide. (A yield of 1000 counts in the underlying metal corresponds to 0.15%, illustrating the matrix effect for Cl ion yields.)

Results

SIMS Profiles of Native Oxides. SIMS profiles of both single crystal and polycrystalline Al are typical for thin native oxides. On single crystals, the native oxide ranges from 3 to 4 nm in thickness, while on polycrystalline films, oxide layers as

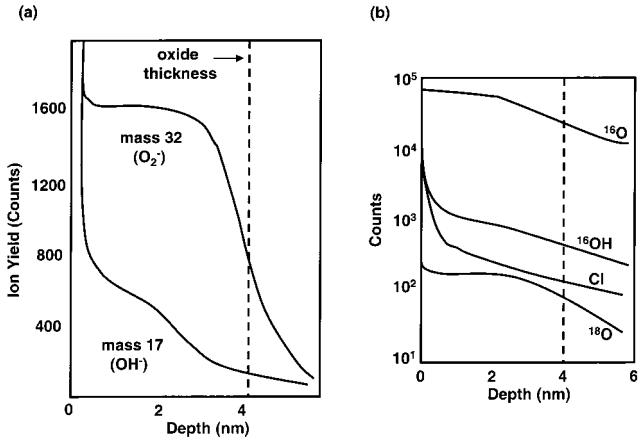

Figure 4. Yields of different sputtered ions vs depth or sputtering time for the native oxide on Al(111). Dashed line indicates the position of the Al:Al_2O_3 interface. (a) Comparisons of the profiles for mass 32 (which like mass 16 is used to detect the presence of the oxide) and mass 17 (which is due to hydroxide). (b) Logarithm of sputtering yield vs depth for several key anions. For this sample, the "bulk" value of the ^{16}O "internal reference" signal of 6×10^4 counts means that all other yields need to be multiplied by a factor of 1.7 ($10^5/6 \times 10^4$) to convert counts into concentration units using the ERD or RBS standards. Here, the corrected ion yield for mass 17 is around 2000 counts, which corresponds to a bulk hydroxide content of 0.7%.

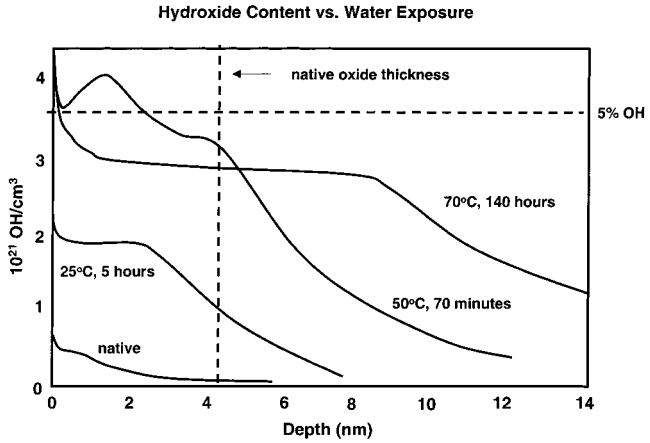

Figure 5. Hydroxide profiles (mass 17 + mass 18) for evaporated Al film on Si immersed in D_2O for the times and temperatures indicated. The vertical dashed line indicates the thickness of the native oxide prior to water exposure (based on mass 16 profile), while the horizontal dashed line indicates the hydroxide concentration at which 5% of the oxygens present are protonated.

thick as 6 nm have been observed. All native oxides examined to date exhibit significant hydroxide ion concentrations (Figure 4a). All profiles show high hydroxide concentrations at the immediate surface (the top nanometer). Sometimes the hydroxide concentration decreases with depth relative to the oxygen concentration all the way to the Al_2O_3:Al interface. In other native oxides, the hydroxide content is relatively constant with depth. The profile for a polycrystalline Al sample shown in Figure 4a represents an intermediate case where the hydrated layer appears to be thinner than the native oxide (as indicated by O^- or O_2^- profiles). Regardless of the profile shape, the hydroxide content in the midpoint of the oxide ranges from 5×10^{20} to 10×10^{20} OH/cm^3. This means that 1−2% of the oxygens present are protonated. Although the native oxides are unlabeled, a mass 18 profile is observed corresponding to $^{18}O^-$. The mass 18:mass 16 sputtering yield ratio of 0.2% corresponds exactly to the natural isotopic abundance of ^{18}O.[24] Conversely, the mass 17 signal is known to correspond to OH^- and not $^{17}O^-$ because the observed mass 17:mass 16 ratio is much greater than the ^{17}O natural abundance of 0.04%.

The sputtering yields for F^- (mass 19, not shown) and Cl^- (mass 35) decrease continuously relative to the O^- signal, indicating that both ions are present as surface contaminants (Figure 4b). The Cl^- yield drops from around 3000 normalized counts at the surface (0.14 at. %) to around 150 counts (6×10^{-3} at. %) near the Al_2O_3:Al interface. However, the observed profile probably reflects the depth resolution of the SIMS rather than representing actual concentration gradients. The bulk Cl^- concentration in the oxide is probably less than 6×10^{-3} at. %. However, while low in an absolute sense, chloride concentrations could still be high enough to influence defect chemistry. Fluoride concentrations could also be significant. However, absolute fluoride concentrations have yet to be determined due to a lack of appropriate calibration standards.

Hydration of Al in the Absence of Applied Potentials. SIMS profiles obtained on "native" polycrystalline aluminum films immersed in deionized D_2O (Figure 5) suggest that hydration may proceed in stages that mirror those reported by Alwitt.[14] In the first stage, hydroxide penetrates the film to the Al_2O_3:Al interface with no appreciable film growth. At the end of stage 1, hydroxide concentrations throughout the film are constant rather than decreasing with depth (see Figure 5, 25 °C, 5 h). At room temperature, the first stage is over in less than 1 h, reaching a steady state in which around 5% of the oxygens are protonated (a 4-fold increase relative to the native oxide). In the second stage of hydration, the oxide starts to thicken with time. At room temperature, the oxide thickness increases from 4.5 nm up to 5 nm (just outside the experimental depth resolution) after 5 h.

Film growth is much more apparent for films exposed to hot water. The oxide on the sample exposed at 50 °C for 70 min is 7 nm thick and has a hydroxide content of almost 15%. The effective diffusion coefficient ($D = (\Delta x)^2/t$, where Δx is the change in film thickness and t is the time in seconds) consistent with the observed film growth is 2×10^{-17} cm^2/s. Hydration at 71 °C for 140 h produces an oxide film that is 14 nm thick (triple the native oxide thickness). The effective diffusion coefficient for film growth at 71 °C of 7×10^{-18} cm^2/s is actually smaller than that seen at 50 °C. Two factors could contribute to slower apparent growth rates in the hottest water. First, film dissolution may be more pronounced in the hotter water, leading to a thinning of the films. Based on the pH (near 6) and the temperature, up to 10 nm of the film could dissolve before the solution becomes saturated with dissolved aluminum hydrolysis products. This would mean that the total thickness of oxide produced could have been as high as 24 nm, leading to a calculated diffusion coefficient of 2×10^{-17} cm^2/s (similar to that seen at 50 °C). However, it appears that the decrease in film growth rate is primarily due to the decrease in the hydroxide content in the oxide (10% at 71 °C compared to the 15% seen at 50 °C). The effect of hydroxide content on the corrosion rate is described in more detail below. Regardless of what stages are present, the rate of film growth is much slower than suggested by earlier reports. For the sample heated at 71 °C for 140 h, the oxide thickness of 14 nm is over 100 times thinner than the 1.5−2.5 μm predicted on the basis of Alwitt's results.[14]

Isotopic Labeling Studies. Isotopic labeling studies have been conducted to obtain estimates for both hydrogen and oxygen migration within the passive film. SIMS results indicate that proton migration is relatively rapid. Profiles obtained for films hydrated in D_2O and transferred through air into the SIMS vacuum system typically exhibit higher yields for −OH than

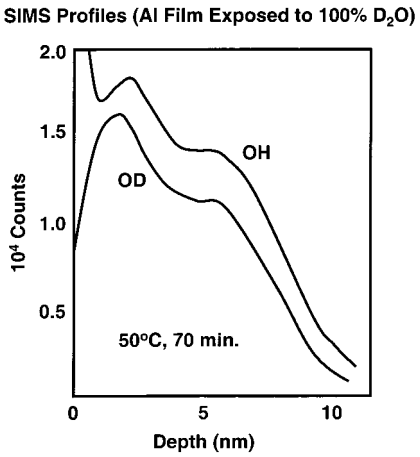

Figure 6. SIMS profiles for mass 17 and mass 18 for a polycrystalline Al sample exposed to 100% D_2O for 70 min at 50 °C showing the extent of H:D exchange observed during atmospheric transfer into the SIMS vacuum chamber.

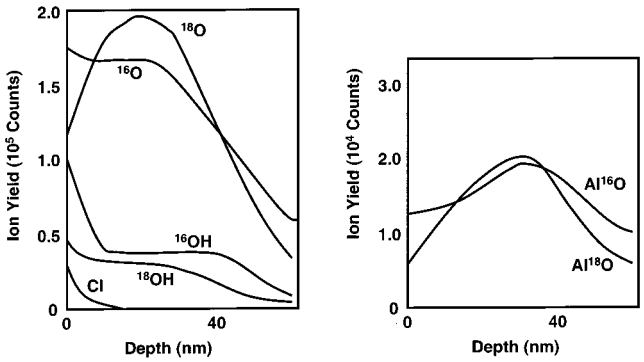

Figure 7. SIMS profiles for the "native" oxide formed by sputter cleaning of the Al(111) crystal followed by reoxidation in 100% O_2. The sample was stored in air for 2 weeks prior to the SIMS analysis.

are seen for −OD (Figure 6). The observed −OH:-OD ratio appears to be related to the extent of exchange between the samples and atmospheric moisture. Even for the fastest transfers, in which the time between the removal of the sample from the solution until the SIMS vacuum system is pumped out is several minutes, only 60−70% of the total hydroxyl concentration is represented by −OD rather than −OH. The ratio of −OH:-OD is always constant with depth, indicating that the effective diffusion coefficient for H:D exchange is at least 5×10^{-18} cm^2/s. Based on the net extent of exchange and estimated transfer times, the results are consistent with an effective diffusion coefficient for D:H exchange within the passive film on the order of 10^{-16}−10^{-17} cm^2/s. (For more rapid exchange, the −OD signal would always be negligible.)

More quantitative estimates have been obtained for reaction rates and diffusion coefficients for O-containing species involving ^{18}O-labeled oxides on Al(111). These results also illustrate that reaction rates and transport are dependent on the history and defect chemistry of the native oxide. SIMS profiles of the "native" ^{18}O-labeled oxide show that it exchanges oxygen with laboratory air after several weeks of storage, as evidenced by the fact that it contains almost as much ^{16}O as ^{18}O (Figure 7). The labeled oxide also exhibits the highest OH content of any native oxide examined to date (almost 20% of the oxygens are protonated). Both of the above observations suggest that the freshly prepared ^{18}O sample is more defective than typical thermal oxides. Immersion of the sample in D_2O at room temperature results in a thickening of the oxide from the native value of around 4.5 nm to 8.5 and 11 nm after 3 h and 25.5 h,

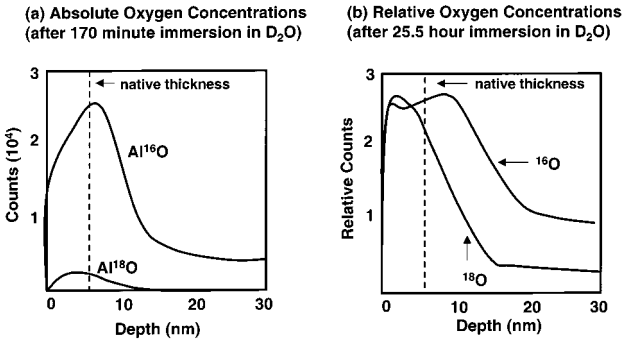

Figure 8. SIMS profiles of ^{18}O-labeled Al(111) surface after exposure to room-temperature D_2O. Dashed lines indicate thickness of native oxide prior to immersion in water. (a) Profiles for $Al^{18}O$ and $Al^{16}O$ after 170 min immersion. (b) Profiles for ^{16}O and ^{18}O scaled to give similar surface concentrations after immersion for 25.5 h. Actual ^{18}O counts are approximately 10% of the ^{16}O counts.

respectively. This rate of layer growth is 5−10 times faster than seen for standard native oxides. Interestingly, the hydroxide content of the film appears to decrease slightly as a function of immersion time in water from the "native" value of OH/O = 19% to 13% after 25.5 h. This suggests that the rate of hydroxide condensation can sometimes exceed the rate of oxide hydrolysis within the film, promoting the "healing" of hydroxide defects. It appears that competition between hydration and dehydration reactions cause all oxides on aluminum to gravitate toward the same hydroxide concentrations when immersed in water regardless of the initial hydroxide or defect concentrations (see Discussion).

The use of the ^{18}O label reveals several new features regarding the hydration process (Figure 8). First, although water exposures result in only a slight film thickening, oxygen exchange between the water and the oxide is extensive. The ^{18}O:^{16}O ratio in the outer portion of the oxide drops from 1.1 to 0.2 and to 0.1 after immersion in room temperature water for 3 h and 25.5 h, respectively (Figure 8a). Assuming that the exchange near the surface reflects the rate constant for reversible hydrolysis, an oxygen exchange rate on the order of 2×10^{-3} s^{-1} is indicated. For the sake of comparison, this exchange rate is 500 times slower than the measured rate at which coordinated water molecules exchange in the inner coordination sphere around dissolved Al^{3+} ions.[25] Second, a comparison of the relative ^{18}O and ^{16}O concentrations with depth (Figure 8b) shows that the ^{18}O marker layer, although slightly thicker than the native oxide, is located on top of an ^{16}O-labeled zone that is essentially ^{18}O-free. The marker layer position and thickness suggest that oxygen diffusion is faster than aluminum diffusion through the passive film and that film dissolution is negligible (at least at room temperature). The effective diffusion coefficient calculated for oxygen is near 10^{-17} cm^2/s. The diffusion coefficient for O is comparable to that inferred for H. The extent of ^{16}O:^{18}O exchange is also comparable to that seen in H:D exchange. Although more quantitative measurements will be required to make a definitive conclusion, the results to date imply that either −OH or water is the mobile species in the oxide and that O and H diffusion are coupled.

The results obtained on the ^{18}O-labeled sample indicate that oxygen diffusion in passive oxides is accelerated by the presence of hydroxide ions, allowing limited reaction between the underlying Al and water to occur. Assuming that film growth is diffusion controlled, that the diffusion coefficient is constant with time, and that the rate of film dissolution is negligible, the room temperature results suggest that the log of the effective diffusion coefficient is roughly proportional to the hydroxide

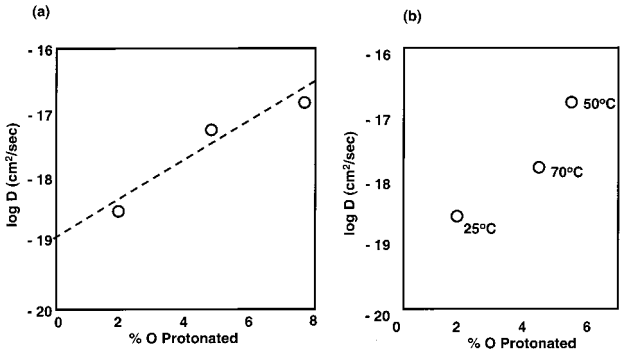

Figure 9. Effective diffusion coefficient for film growth (based on extent of film growth vs $t^{1/2}$) for aluminum oxide films as a function of average hydroxide content. (a) Results obtained at room temperature. The two "wettest" samples were labeled with ^{18}O. (b) Results obtained on polycrystalline Al at different temperatures.

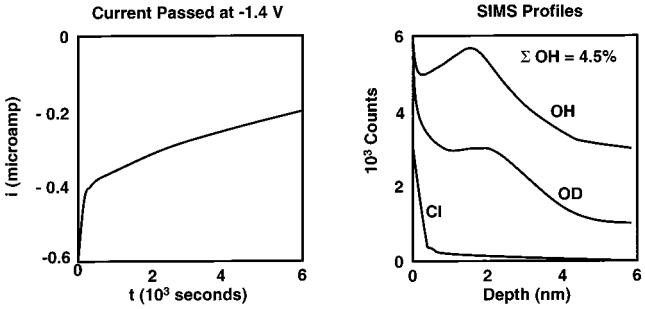

Figure 10. Results obtained for cathodic polarization of polycrystalline Al sample. (a) Current passed as a function of time at an applied voltage of −1.4 V vs Pt pseudoreference electrode. (b) SIMS profiles for the same sample at the end of the polarization experiment (t = 6000 s).

content (Figure 9a). The variable temperature results show a similar trend, where film growth appears to be slower at 70 °C than it is at 50 °C due to a decrease in the hydroxide content (Figure 9b). While these results are qualitative (due to probable breakdowns in the simplifying assumptions used to estimate the diffusion coefficients), it is clear that diffusion coefficients within the passive film are not constant but can vary by orders of magnitude depending on the hydroxide concentration.

Hydration of Al Under Cathodic Polarization. SIMS analyses were performed on a polycrystalline Al sample that was immersed in a D_2O:$H_2{}^{18}O$ mixture containing 0.05 M KCl under cathodic polarization (E = −1.4 V, i = 0.3 mA, t = 5000 s)(Figure 10). With cathodic polarization, anionic species in the film should be driven from the Al to the solution, while cationic species should be driven from solution toward the Al. The total current passed through the sample is sufficient either to dissolve 2 nm of the oxide film or to generate 2×10^{-8} mol of H_2 via the reactions:

$$Al_2O_3 + 3H_2O + 6e^- \rightarrow 2Al + 6OH^- \quad (1)$$

$$2H_2O + 2e^- \rightarrow H_2 + 2OH^- \quad (2)$$

Experimental results suggest that both oxide dissolution and H_2 evolution reactions occur. The apparent film thickness of the cathodically polarized film is less than that of the native oxide (3.5 nm vs 5.0 nm). However, gas evolution (presumed to be hydrogen) was also observed while the voltage was applied. The hydrogen contents of cathodically polarized films are similar to those seen in oxides in the absence of any polarization (8% of the oxygens are protonated after 1.4 h of immersion at −1.4 V.) The chloride ion profiles fall within the range seen for native

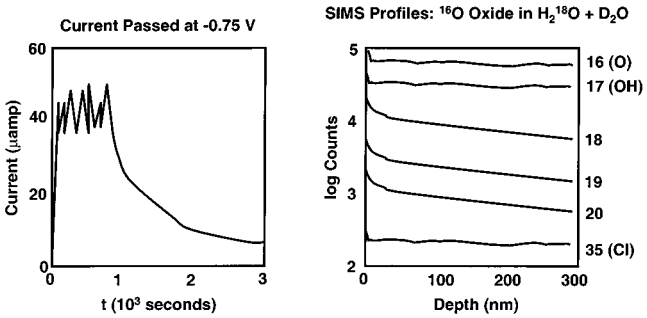

Figure 11. Results obtained for anodic polarization of polycrystalline Al sample. (a) Current passed as a function of time at an applied voltage of −0.75 V vs Pt pseudoreference electrode. (b) SIMS profiles for the same sample after polarization for 3000 s.

samples. If chloride ions are being swept toward the surface under the influence of cathodic polarization, the motion is masked by the decaying SIMS signal associated with the removal of surface chloride contamination.

Hydration of Al Under Anodic Polarization. The ideal SIMS experiments for evaluating pitting mechanisms involve anodically polarizing Al samples at potentials that are slightly above and below the pitting potential. Unfortunately, our Al samples were not as well behaved under anodic polarization as they were under cathodic polarization. Current−voltage curves were highly irreproducible, with open circuit potentials, apparent pitting potentials, and measured currents at a particular potential being highly dependent on prior sample history. Attempts at identifying the pitting potential based on short-time cyclic voltammagrams failed. SIMS results to date have been obtained at potentials of from −0.95 to −0.75 V. While these voltages are well above the pitting potential (based on current magnitude and current spikes (Figure 11a), the absolute value of the pitting potential is unknown and may not be the same for each sample.

The behavior of the passive film above the pitting potential is dramatically different from hydration observed under any other conditions tested to date (Figure 11b). First, film growth is extensive and rapid. Anodic films examined have all been too thick to sputter through using standard sputtering conditions in the SIMS apparatus. If it is assumed that all of the electrochemical currents passed are associated with the oxidation of Al (reverse of eq 7), calculated film thicknesses range from 0.1 to 0.2 μm. A second unique feature of the anodically polarized films is high hydroxide concentrations. The fraction of oxygens converted to hydroxide range from 50% to 75% for applied voltages ranging from −0.75 to −0.95 V, with lower anodic potentials (e.g., −0.95 V) resulting in higher hydroxide concentrations. At the low end, the observed hydroxide contents are consistent with the presence of boehmite (AlOOH), which would have a hydroxide content of 50%. Higher hydroxide contents suggest that either molecular water is present within the boehmite film, or that a mixture of boehmite and $Al(OH)_3$ is present. X-ray diffraction analyses do not resolve what phases are present, as the films appear to be amorphous.

The anodized films sometimes contain high, uniform concentrations of chloride ions. The maximum Cl signal detected was for a sample anodized at −0.75 V, which had a normalized Cl count of 2500 (relative to 300 for the native oxide). This maximum chloride content is around 0.1 at. % based on the ion implanted calibration standard. However, such high concentrations were not observed for samples that were carefully rinsed in deionized water (showing uniform concentrations of from 100 to 300 counts, similar to the native oxide). The Cl results suggest that chloride ions occupy sites that are accessible

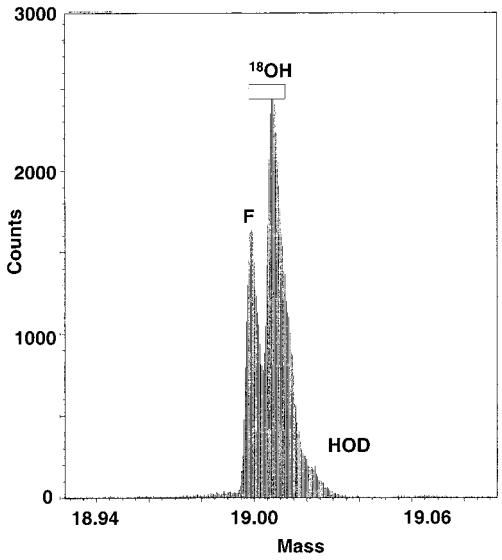

Figure 12. High mass resolution data for the ^{18}O-labeled oxide after 170 min of exposure to water at room temperature. The data represent results collected for a single sputtering time, representing a point deep into the depth profile. The results show the contributions to the "mass 19" peak due to F, ^{18}OH, and HOD. Although the counts due to F are high, actual fluoride concentrations are probably quite low, as the sputtering yield for F is probably at least 10 times higher than that for OH.

to water. It appears that the chloride ions are present as physisorbed anions in a porous oxide film rather than being incorporated into a homogeneous oxide structure as dopants that are chemically bound to Al.

The ability of water to readily penetrate the anodic films is indicated by the behavior of different mass peaks in samples exposed to water containing D and ^{18}O. Although the ion yield associated with $-$OH (mass 17) is constant with depth, the yields for masses 18, 19, and 20 decrease with depth. If the signals for the heavier species were due entirely to hydroxide ions (such as $-$OD, $-^{18}$OH, and $-^{18}$OD), the depth profiles should mirror the mass 17 ($-$OH) signal. The fact that they do not suggests that other species, including water (as H_2O, HDO, $H_2{}^{18}O$) and F$-$ could be contributing to the ion signal. To check this possibility, an isotopically resolved scan was made for one data point corresponding to mass 19 (Figure 12). The results show that while most of the signal is due to $-^{18}$OH, significant concentrations of F$-$ and HDO are present. It appears that the concentration gradients in the mass 18$-$20 signals are associated with water that was entrapped in the oxide and that diffuses outward in the SIMS vacuum environment.

Discussion

While thermal oxide films are excellent at passivating Al surfaces, the SIMS results clearly show that the films are neither "passive" nor inert. It is an oversimplification to view the thermal oxide as a rigid and unchanging structure through which low concentrations of aluminum and oxygen vacancies migrate. Reversible hydrolysis reactions are continually taking place at the oxide:water interface. Surface hydroxide and/or oxide ions replaced at the surface are free to exchange with subsurface oxide ions via diffusion. While both the surface exchange and diffusion processes are relatively slow, the passive film is so thin that there is complete oxygen exchange between the oxide and water after only a day at room temperature. Given the level of oxygen exchange, it is clear that any phenomena that can influence either the forward or reverse hydration reactions could have a profound effect on the corrosion of aluminum. Adsorption of anions such as the chloride ion in the electrical double layer is one factor that could potentially influence such processes. However, systematic experiments regarding the role of chloride ion in mediating reversible hydrolysis have yet to be conducted.

Although reversible hydration is happening all the time, the steady state concentration of hydroxide ions is normally low, at least relative to the hydrated oxyhydroxide or hydroxide phases. Measured hydroxide concentrations range from 0.5% (for air-exposed native oxides) to 15% (after days of exposure to hot water) of the total oxygen in the film compared with 50% for AlOOH, or 100% for $Al(OH)_3$. The maximum hydroxyl content for samples exposed to water is comparable to the 12.5% OH expected for HAl_5O_8, which is predicted to be the most stable hydrated form of the spinel phase γ-Al_2O_3. Regardless of what phase is present, it is important to note that the OH concentrations (and inferred Al-vacancy concentrations) are many orders of magnitude higher than the Al$-$ or O$-$ vacancy concentrations in α-Al_2O_3 and could clearly contribute to observed corrosion and pitting phenomena.

The hydroxide concentration within the passive film adjusts to environmental changes within a relatively short period of time. Under water, the films tend to hydrate. Films stored under dry conditions tend to dehydroxylate with time. The SIMS results indicate that highly defective films can lose hydroxide ions even when stored under water. The results suggest that under a given set of environmental conditions, passive films gravitate toward the same hydroxide concentration regardless of their initial composition. One possible explanation for this phenomenon is that reversible hydrolysis and condensation reactions occur until specific hydrated phases are produced. For normal hydration, the phase to which films gravitate appears to be HAl_5O_8. For anodic polarization, the most stable phase appears to be AlOOH.

The SIMS results suggest that ionic transport and diffusion ($D = 10^{-19}-10^{-17}$ cm^2/s) through passive films is fast enough to account for the kinetics of both corrosion and pitting. It is clear that ionic transport in the native oxide is much more rapid than it is in bulk α-Al_2O_3. In addition, it is clear that the presence of hydroxide ions influence both ion migration and corrosion rates. The isotopic labeling studies suggest that even if a phase such as γ-Al_2O_3 is present, which contains high aluminum vacancy concentrations, oxygen transport is rapid relative to aluminum transport. It appears that hydroxide ions facilitate this oxygen transport. Enhanced transport appears to explain why the rate at which native oxides grow in water increases dramatically as the hydroxide concentration in the oxide increases (Figure 9). However, the hydroxide content of the oxide can either increase or decrease with time depending on the relative rates of several key reactions. On bulk Al_2O_3, the processes are limited to hydrolysis (to form hydroxyl groups), condensation (which consumes hydroxyl groups), and subsurface diffusion. For the passive films on Al, there is the additional process of hydroxide removal involving redox reactions at the Al_2O_3:Al interface to produce H_2. Such reactions may make hydration of the passive film self-limiting. Hydration leads to enhanced transport, but enhanced transport leads to faster annihilation of hydroxide at the Al_2O_3:Al interface. The final hydroxide content and film thickness may reflect the balance of these two competing processes.

The role of applied voltages in influencing hydration and defect migration has yet to be determined on a mechanistic level. The SIMS results suggest that under cathodic polarization, the

dominant species migrating through the film are electrons that reduce water to H_2 and promote limited oxide dissolution. Under anodic polarization, it is clear that extensive hydration and film thickening occur. However, because studies to date have been limited to polarizations above the pitting potential, it is not clear how the films form. Observed films could have been produced as a result of uniform and highly accelerated hydroxide transport through the passive film or as a result of a reprecipitation process associated with high solution concentrations produced as a result of localized pitting. Further experiments involving the use of labeled oxides, a range of electrolytes (e.g., chloride vs nitrate), and a range of anodic polarization conditions (particularly below the pitting potential) will be required to discriminate between these possibilities.

Summary

Corrosion and pitting of Al are complex processes that are mediated by a dynamic oxide film whose composition and properties are variable with time and environmental conditions. The major implication of the SIMS results reported here is that hydration of the passive film plays an important role in mediating the properties of passive oxide films.

Depth profiles obtained with the use of isotopic labels suggest that

1. The hydroxide content of the amorphous oxide layer on Al is higher than the concentration of any other known defect, ranging from a few atomic percent in air to as much as 15 at. % for samples immersed in water.

2. The native oxide is a dynamic structure in which Al−O bonds are constantly being broken and re-formed by reversible hydrolysis reactions that add and remove hydroxide ions from the lattice. Such reactions lead to extensive scrambling of labeled oxygen between water and the oxide film.

3. The isotopic labeling experiments suggest that H and O have comparable diffusion coefficients ($D = 10^{-16}-10^{-17}$ cm^2/s) in hydrated native oxides. The results suggest that hydroxide ions (or water molecules) are the mobile species in the films (rather than H^+, O^{2-}, or Al^{3+}) and that transport rates are sufficiently rapid to account for the kinetics of Al corrosion and pitting processes.

Hydration and transport processes in the native oxide appear to be coupled with higher hydroxide concentrations, leading to faster transport. Extensive experimentation will be required to deconvolute the contributions of different hydration, dehydration, and transport processes to the overall behavior of the passive film. Knowledge of the rates and energetics of elemental steps in film hydration will be required to develop quantitative models for predicting the kinetics of corrosion and pitting for active metals such as aluminum. It is hoped that the SIMS results reported here will stimulate further research that will allow for the determination of such rate constants.

Acknowledgment. Funding for this work was provided by the Materials Sciences Division of the Office of Basic Energy Sciences. Sandia is a multiprogram laboratory operated by Sandia Corp., a Lockheed Martin Co., for the United States Department of Energy under Contract DE-ACO4-94AL85000. A portion of this research was performed in the Environmental Molecular Sciences Laboratory, a national scientific user facility located at Pacific Northwest National Laboratory and sponsored by the Department of Energy's Office of Biological and Environmental Research. We dedicate this paper to Jerry Nelson, who is retiring after over thirty years of surface science research in the National interest.

References and Notes

(1) Szklarska-Smialowska, Z. *Corrosion* **1971**, *27*, 223.

(2) Bockris, J. O'M.; Minevski, L. V. *J. Electroanal. Chem*. **1993**, *349*, 375.

(3) Chao, C. Y.; Lin, L. F.; Macdonald, D. D. *J. Electrochem Soc.* **1981,** *128*, 1187.

(4) Macdonald, D. D. *J. Electrochem. Soc.* **1992**, *139*, 3434.

(5) Prot, D.; Monte, C. *Philos. Magn. A* **1996**, *73*, 899.

(6) Le Gall, M.; Huntz, A. M.; Lesage, B.; Monty, C.; Bernardini, J. *J. Mater. Sci.* **1995**, *30*, 201.

(7) Pells, G. P.; Hodgson, E. R. *J. Nucl. Mater*. **1985**, *226*, 286.

(8) Sohlberg, K.; Pennycook, S. J.; Pantelides, S. T. *J. Am. Chem. Soc.* **1999**, *121*, 7493.

(9) Sullivan, J. P.; Barbour, J. C.; Dunn, R. G.; Son, K. A.; Montez, L. P.; Missert, N.; Copeland, R. G. *Electrochem. Soc. Proc*. **1999**, *98*, 111.

(10) Kreuer, K.-D. *Chem. Mater*. **1996**, *8*, 610.

(11) Wefers, K.; Bell, G. M. Oxides and Hydroxides of Aluminum. Technical Paper No 19; Alcoa Research Laboratories, 1972.

(12) Arjona, A. M.; Fripiat, J. J. *Trans. Faraday Soc.* **1967**, *63*, 2936.

(13) Jaccard, C. Transport Properties of Ice. In *Water and Aqueous Solutions*; Horne, R. A., Ed.; Wiley-Interscience: New York, 1972; pp 25−65.

(14) Alwitt, R. S. The Aluminum-Water System. In *Oxides and Oxide Films*; Diggle, J. W., Vijh, A. K., Eds.; Marcel Dekker: New York, 1976; Chapter 3.

(15) Pourbaix, M. *Atlas of Electrochemical Equilibria*; National Association of Corrosion Engineering: Houston, TX, 1974.

(16) Paul, J.; Hoffmann, F. M. *J. Phys. Chem*. **1986**, *90*, 5321.

(17) Kobayashi, M.; Niioka, Y. *Corrosion Sci*. **1990**, *31*, 237.

(18) Song, W.; Du, J.; Xu, Y.; Long, B. J. *Nucl. Mater*. **1997**, *246*, 139.

(19) Cox, D. F.; Hoflund, G. B.; Hocking, W. H. *Appl. Surf. Sci*. **1986**, *26*, 239.

(20) Mitchell, D. F.; Graham, M. J. *J. Electrochem. Soc*. **1986**, *133*, 937.

(21) Haneda, H.; Sakaguchi, I.; Watanabe, A.; Tanaka, J. *Defect and Diffusion Forum* **1997**, *143*−*147*, 1219.

(22) Thevuthasan, S.; Baer, D. R.; Engelhard, M. H.; Liang, Y.; Worthington, J. N.; Howard, T. R.; Munn, J. R.; Rounds, K. S. *J. Vac. Sci. Technol. B* **1995**, *13*, 1900.

(23) Baer, D. R.; Windisch, C. F.; Engelhard, M. H.; Danielson, M. J.; Jones, R. H.; Vetrano, J. S. *J. Vac. Sci. Technol. A* **2000**, *18*, 131.

(24) Weast, R. C., Ed., *CRC Handbook of Chemistry and Physics*; CRC Press: Cleveland, OH, 1977; p B-272.

(25) Cotton, F. A.; Wilkinson, G. *Advanced Inorganic Chemistry*; Interscience: New York, 1972; p 656.